

Resonantly damped oscillations of elliptically shaped stratified emerging coronal loops

K. Karami^{1*}, S. Amiri^{1†}, K. Bahari^{2‡}, Z. Ebrahimi^{1§}

¹Department of Physics, University of Kurdistan, Pasdaran Street, Sanandaj, Iran

²Physics Department, Faculty of Science, Razi University, Kermanshah, Iran

June 26, 2018

Abstract

The effects of both elliptical shape and stage of emergence of the coronal loop on the resonant absorption of standing kink oscillations are studied. To do so, a typical coronal loop is modeled as a zero-beta longitudinally stratified cylindrical magnetic flux tube. We developed the connection formulae for the resonant absorption of standing transversal oscillations of a coronal loop with an elliptical shape, at various stages of its emergence. Using the connection formulae, the dispersion relation is derived and solved numerically to obtain the frequencies and damping rates of the fundamental and first-overtone kink modes. Our numerical results show that both the elliptical shape and stage of emergence of the loop alter the frequencies and damping rates of the tube as well as the ratio of frequencies of the fundamental and its first-overtone modes. However, the ratio of the oscillation frequency to the damping rate is not affected by the tube shape and stage of its emergence and also is independent of the density stratification parameter.

Key words: Sun: corona — Sun: magnetic fields — Sun: oscillations

*KKarami@uok.ac.ir

†Sirwanamiri@yahoo.co.uk

‡K.Bahari@razi.ac.ir

§zanyar.ebrahimi@gmail.com

1 Introduction

Solar corona and its extraordinary high temperature has been the topic of various debates and studies from several decades ago. The origin and the source of coronal continual heating and high temperature have been related to coronal loops. The claim that the coronal loops and their behaviors such as their damping oscillations may be one of the main reasons of coronal heating, has been investigated through several studies so far.

Transverse oscillations of coronal loops have been observed by the Transition Region and Coronal Explorer (TRACE) for several years (see e.g. Aschwanden et al. 1999; Schrijver & Brown 2000). Nakariakov et al. (1999) interpreted these oscillations as fast kink modes with the period ranging from 2.3 to 10.8 min and decay time from 3.2 to 20.8 min. The observed values of the periods and decay times make it possible to obtain indirect information on the conditions of the plasma and magnetic field in coronal loops.

Ofman & Aschwanden (2002) used the data deduced by Aschwanden et al. (2002) to investigate the oscillations of 11 coronal loops. They argued that the observed TRACE loops consist of multiple unresolved thin loop threads which produce inhomogeneous internal structure of the observed loop. They adopted 1-dimensional cartesian slabs of plasma with the magnetic field lines in the z -direction and the direction of the inhomogeneity along the x -axis normal to the magnetic surfaces, as a simple model for the oscillating loops. They found that the dependence of the decay time on both the length L and the width w of the loop is in excellent agreement with the power law damping predicted by phase mixing.

The property of resonant absorption as a non-thermal mechanism makes it possible to describe the heating of magnetic loops in solar corona as well as rapid decaying of magnetohydrodynamics (MHD) waves even in weakly dissipative plasmas (see e.g. Ionson 1978; Poedts et al. 1989; Ofman et al. 1994; Erdélyi & Goossens 1994, 1995; Tirry & Goossens 1996; Andries et al. 2005b; Safari et al. 2006; Dymova & Ruderman 2006; Goossens et al. 2009).

Verwichte et al. (2004), using the observations of TRACE, have identified the fundamental and its first harmonic of the transverse kink mode in two coronal loops. The period ratios observed by Verwichte et al. (2004) are 1.81 ± 0.25 and 1.64 ± 0.23 . However, these values were corrected with the improvement of the observational error bars to 1.82 ± 0.08 and 1.58 ± 0.06 , respectively, by Van Doorselaere et al. (2007). Also Verth et al. (2008) added some further corrections by considering the effects of loop expansion and estimated a period ratio of 1.54. All these values clearly are lower than 2. This may be caused by different factors such as the effects of density stratification (see e.g. Andries et al. 2005a; Erdélyi & Verth 2007; Karami & Asvar 2007; Safari et al. 2007; Karami et al. 2009) and magnetic twist (see Erdélyi & Carter 2006; Erdélyi & Fedun 2006; Karami & Barin 2009; Karami & Bahari 2010, 2012) in the loops.

Karami et al. (2009, hereafter Paper I) investigated the effect of longitudinally stratification on resonant absorption of MHD waves for both kink ($m = 1$) and fluting ($m = 2$) modes. They found that the frequencies and damping rates of both the fundamental and first-overtone modes increase when the stratification parameter increases. Also for stratified loops they obtained the ratio of the frequencies ω_2/ω_1 of the first overtone and its fundamental mode less than 2.

Morton & Erdélyi (2009) studied the effects of both the elliptical shape and stage of emergence of the loops on the period ratio P_1/P_2 for the minor and major elliptical cases. Their results showed that the parameter characterising the stage of emergence does affect the value of period ratio P_1/P_2 . Particularly, the greatest contribution from emergence to the period ratio occurs when the loop is fully emerged. Also they showed that the ellipticity of the loop has an important role in the value of P_1/P_2 for minor elliptical case but the major ellipse was found to have a less effect on the period ratio of standing oscillations.

Here we combine the two models considered in Paper I and Morton & Erdélyi (2009) to investigate of the effects of both elliptical shape and stage of emergence of the coronal loop on the resonant absorption of standing transversal kink oscillations observed by the TRACE. This paper is organized as follows. In Sections 2 and 3, we combine the two techniques of Paper I and Morton & Erdélyi (2009) to derive the equations of motion, introduce the relevant connection formulae and obtain the dispersion relation. In Section 4, we give numerical results. Section 5 is devoted to conclusions.

2 Equations of motion and modeling of the flux tube

The linearized MHD equations for a zero-beta plasma are given by

$$\frac{\partial \delta \mathbf{v}}{\partial t} = \frac{1}{4\pi\rho} \{(\nabla \times \delta \mathbf{B}) \times \mathbf{B} + (\nabla \times \mathbf{B}) \times \delta \mathbf{B}\} + \frac{\eta}{\rho} \nabla^2 \delta \mathbf{v}, \quad (1)$$

$$\frac{\partial \delta \mathbf{B}}{\partial t} = \nabla \times (\delta \mathbf{v} \times \mathbf{B}) + \frac{c^2}{4\pi\sigma} \nabla^2 \delta \mathbf{B}, \quad (2)$$

where $\delta \mathbf{v}$ and $\delta \mathbf{B}$ are the Eulerian perturbations of velocity and magnetic fields; \mathbf{B} , ρ , σ , η and c are the background magnetic field, the mass density, the electrical conductivity, the viscosity and the speed of light, respectively.

The simplifying assumptions are the same as in Karami & Asvar (2007). According to Andries et al. (2005b) and Paper I, one can expand the perturbed quantities $\delta \mathbf{v}$ and $\delta \mathbf{B}$ as follows

$$\begin{aligned} \delta \mathbf{B}(r, z) &= \sum_{k=1}^{\infty} \delta \mathbf{B}^{(k)}(r) \psi^{(k)}(z), \\ \delta \mathbf{v}(r, z) &= \sum_{k=1}^{\infty} \delta \mathbf{v}^{(k)}(r) \psi^{(k)}(z), \end{aligned} \quad (3)$$

where $\psi^{(k)}(z)$ s form a complete set of orthonormal eigenfunctions and satisfy the eigenvalue relation

$$L_A \psi^{(k)} = \zeta_k \psi^{(k)}, \quad (4)$$

where L_A is the Alfvén operator,

$$L_A = \rho \omega^2 + \frac{B^2}{4\pi} \frac{\partial^2}{\partial z^2} = \rho \left(\omega^2 + v_A^2 \frac{\partial^2}{\partial z^2} \right), \quad (5)$$

with Alfvén velocity $v_A = \frac{B}{\sqrt{4\pi\rho}}$ and straight constant background magnetic field $\mathbf{B} = B\hat{\mathbf{z}}$.

We further assume there is a density stratification along the tube axis in z -direction. Since we are interested in resonantly damped oscillations, it implies that the density profile must be radially structured too. Following Paper I, we consider the density profile given by

$$\rho(r, z) = \rho_0(r) \rho(z), \quad (6)$$

where

$$\rho_0(r) = \begin{cases} \rho_{\text{in}}, & (r < R_1), \\ \left[\frac{\rho_{\text{in}} - \rho_{\text{ex}}}{R - R_1} \right] (R - r) + \rho_{\text{ex}}, & (R_1 < r < R), \\ \rho_{\text{ex}}, & (r > R). \end{cases} \quad (7)$$

Here, R is the loop radius and $R_1 < R$ is the radius of the homogeneous part of the tube. The radius at which resonant absorption occurs is between R_1 and R . The thickness of the inhomogeneous layer, $l = R - R_1$, will be assumed to be small. Here, ρ_{in} and ρ_{ex} are the footpoint densities of the interior and exterior regions of the tube, respectively.

According to Morton & Erdélyi (2009) we consider two types of elliptical loop that can occur, the minor elliptical loop where minor axis of the ellipse is the vertical axis of the loop, and the major elliptical loop where major axis of the ellipse is the vertical axis of the loop. Note that the minor ellipse is a situation that occurs most plausibly under coronal conditions.

For the minor elliptical case, the longitudinally stratified density profile takes the form

$$\rho(z) = \exp \left(-\mu \frac{\cos(\alpha(z)) [1 - \epsilon^2 \sin^2(\alpha(z))]^{-\frac{1}{2}} - \lambda}{1 - \lambda} \right), \quad (8)$$

and for the major one, it is given by

$$\rho(z) = \exp \left(-\mu \frac{\cos(\alpha(z)) (1 - \epsilon^2)^{1/2} [1 - \epsilon^2 \cos^2(\alpha(z))]^{-\frac{1}{2}} - \lambda}{1 - \lambda} \right), \quad (9)$$

where

$$\epsilon = \left(1 - \frac{b^2}{a^2} \right)^{1/2}, \quad (10)$$

is the ellipticity of the loop with minor half-axis of length b , and major half-axis of length a . Also $\mu := \frac{L}{\pi H}$ is defined as stratification parameter, where H and L are the density scale height and length of the loop, respectively. The parameter λ describes the stage of emergence of the loop from the photosphere. It is defined as the ratio of the distance of the photosphere from center of the ellipse to the vertical half-axis. A positive value of λ refers to the situation in which the center of ellipse is sitting below the photosphere (early stage emergence), and thus, the negative λ for the center above the photosphere (late stage emergence). A zero value of λ corresponds to a loop having a semi-elliptical shape. For the minor elliptical case, λ is given by

$$\lambda = 1 - \frac{\mu H}{b}, \quad (11)$$

where μH is the distance of the loop apex from the photosphere. For the major one, λ is defined as

$$\lambda = 1 - \frac{\mu H}{a}. \quad (12)$$

Note we have considered a tube of length L which its footpoints are in the two points $z = 0$ and $z = L$, and also note that in Eqs. (8) and (9), $\alpha(z)$ is the angle between the vertical axis of the loop and the line joining the center of the ellipse to the plasma element located at distance z along the tube. Following Morton & Erdélyi (2009) for the minor elliptical case, one can obtain the value of $\alpha(z)$ by calculating the ellipse arc length defined as

$$\int_0^{t_1} (1 - \epsilon^2 \sin^2(t))^{\frac{1}{2}} dt = \left(\frac{2z}{L} - 1 \right) \int_0^{t_2} (1 - \epsilon^2 \sin^2(t))^{\frac{1}{2}} dt, \quad (13)$$

where t_1 and t_2 are parametric angles given by

$$t_1 = \arctan\left(\frac{b}{a}\tan(\alpha)\right), \quad t_2 = \arctan\left(\frac{b}{a}\tan(\theta)\right), \quad (14)$$

and

$$\theta = \arctan\left[\frac{1}{\lambda}\left(\frac{1-\lambda^2}{1-\epsilon^2}\right)^{\frac{1}{2}}\right], \quad (15)$$

is the angle between the vertical axis of the loop and a line that joins the ellipse center to the loop foot-point (see Fig. 2 in Morton & Erdélyi 2009).

For the major elliptical case, we have

$$\int_{t_1}^{\frac{\pi}{2}} (1 - \epsilon^2 \sin^2(t))^{\frac{1}{2}} dt = \left(\frac{2z}{L} - 1\right) \int_{t_2}^{\frac{\pi}{2}} (1 - \epsilon^2 \sin^2(t))^{\frac{1}{2}} dt, \quad (16)$$

where

$$t_1 = \arctan\left(\frac{b}{a}\cot(\alpha)\right), \quad t_2 = \arctan\left(\frac{b}{a}\cot(\theta)\right), \quad (17)$$

and

$$\theta = \arctan\left[\frac{\left((1-\epsilon^2)(1-\lambda^2)\right)^{\frac{1}{2}}}{\lambda}\right]. \quad (18)$$

According to Paper I, in the absence of dissipation, in the interior region ($r < R_1$), solutions of Eqs. (1) and (2) are

$$\delta B_z^{(\text{in})}(r, z) = \sum_{k=1}^{+\infty} A^{(\text{in},k)} J_m(|k_{\text{in},k}|r) \psi^{(\text{in},k)}(z), \quad (19)$$

$$\delta v_r^{(\text{in})}(r, z) = -\frac{i\omega B}{4\pi} \sum_{k=1}^{+\infty} \frac{k_{\text{in},k}}{\zeta_{\text{in},k}} A^{(\text{in},k)} J'_m(|k_{\text{in},k}|r) \psi^{(\text{in},k)}(z), \quad (20)$$

where

$$k_{\text{in},k}^2 = \frac{\zeta_{\text{in},k}}{B^2/4\pi}. \quad (21)$$

Here J_m is the Bessel function of the first kind and a prime on J_m and hereafter on each function indicates a derivative with respect to their appropriate arguments. The solutions for the exterior region $r > R$, are the same as equation (20) except that J_m , index "in", and $|k_{\text{in},k}|$ are replaced by K_m , "ex" and $k_{\text{ex},k} = -\frac{\zeta_{\text{ex},k}}{B^2/4\pi}$, respectively, everywhere. Where K_m is the modified Bessel function of the second kind and shows that the wave amplitude vanishes in large distance away from the tube boundary.

3 Boundary conditions, Connection formulae and dispersion relation

In the absence of dissipation effects, an appropriate dispersion relation is obtained by requiring that the solutions for perturbed quantities are continuous at the tube surface. When a dissipative layer is considered, the solutions may experience jumps across the layer. An appropriate relation connecting the solutions of outside and inside the tube, is called the ‘‘connection formulae’’. Following Paper I, the jump across the boundary (resonance layer) for δB_z and δv_r is

$$[\delta B_z] = 0, \quad (22)$$

$$[\delta v_r] = - \sum_{k=1}^{+\infty} \frac{B\tilde{\omega}m^2 \langle \phi^{(\text{in},k)} | \delta B_z^{(\text{in},k)} \rangle}{4r_A^2 \langle \phi^{(\text{in},k)} | L_{A1} | \phi^{(\text{in},k)} \rangle} \phi^{(\text{in},k)}, \quad (23)$$

where

$$L_{A1} = \frac{\partial L_A}{\partial r} \Big|_{r=r_A} = \tilde{\omega}^2 [1 + S_{kk}] \frac{\partial \rho_0(r)}{\partial r} \Big|_{r=r_A}, \quad (24)$$

and

$$\phi^{(\text{in},k)} = \sqrt{\frac{2}{L}} \sum_{j=1}^{+\infty} \phi_j^{(\text{in},k)} \sin\left(\frac{j\pi}{L}z\right), \quad (25)$$

with

$$\phi_j^{(\text{in},k)} = \begin{cases} \frac{k^2 S_{kj}}{\rho_{\text{in}}(1+S_{kk})(j^2-k^2)} & j \neq k \\ 1 & j = k \end{cases}. \quad (26)$$

Here $\phi^{(\text{in},k)}$ satisfies $L_A \phi^{(\text{in},k)} = 0$ and $\tilde{\omega} = \omega + i\gamma$ where γ is damping rate. Also $R_1 < r_A < R$ $R_1 < r_A < R$ is the radius at which the singularity occurs. Note that $l = R - R_1$ is the thickness of the inhomogeneous layer and Davila (1987) showed that in the resonance absorption, however, the damping rate is independent of the dissipation coefficient values. But the resonance layer width scales as $\delta_A \propto (\frac{\nu}{\rho} + \frac{e^2}{4\pi\sigma})^{1/3}$. Karami & Bahari (2010) showed that for the Reynolds $\mathcal{R} = (\frac{R^2 \rho_i}{\nu}) / (\frac{2\pi R}{v_{A1}}) = 560$ and Lundquist $S = (\frac{4\pi\sigma R^2}{c^2}) / (\frac{2\pi R}{v_{A1}}) = 10^4$ numbers given by Ofman et al. (1994), and taking $L = 10^5$ km, $R/L = 0.01$, $a/R = 0.08$, $\rho_{\text{ex}}/\rho_{\text{in}} = 0.1$, and interior Alfvén velocity $v_{A\text{in}} = 2000$ km s⁻¹ for a typical coronal loop, then one can get $\delta_A \simeq 85$ km which is very close to the thickness of the inhomogeneous layer $l \simeq 87$ km. This suggests that one can use the thin boundary approximation which assumes that the thickness of the resonance layer is the same as the inhomogeneous layer width (see also Goossens et al. 2009).

Note that the effects of elliptical shape and stage of emergence of the loop on the resonant absorption appear in jump conditions via the function S_{kj} which is obtained as

$$S_{kj} = \sqrt{\frac{2}{L}} \int_0^L \sin\left(\frac{k\pi}{L}z\right) \ln(\rho(z)) \sin\left(\frac{j\pi}{L}z\right) dz. \quad (27)$$

Substituting the fields of equation (19) and (20) in jump conditions (22) and (23) gives

$$\begin{pmatrix} \Pi_1^{(\text{ex},1)} & -\Pi_1^{(\text{in},1)} & \Pi_1^{(\text{ex},2)} & -\Pi_1^{(\text{in},2)} & \dots \\ \Xi_1^{(\text{ex},1)} & \Xi_1^{(\text{in},1)} + \mathcal{D}_1^{(\text{in},1)} & \Xi_1^{(\text{ex},2)} & \Xi_1^{(\text{in},2)} + \mathcal{D}_1^{(\text{in},2)} & \dots \\ \Pi_2^{(\text{ex},1)} & -\Pi_2^{(\text{in},1)} & \Pi_2^{(\text{ex},2)} & -\Pi_2^{(\text{in},2)} & \dots \\ \Xi_2^{(\text{ex},1)} & \Xi_2^{(\text{in},1)} + \mathcal{D}_2^{(\text{in},1)} & \Xi_2^{(\text{ex},2)} & \Xi_2^{(\text{in},2)} + \mathcal{D}_2^{(\text{in},2)} & \dots \\ \vdots & \vdots & \vdots & \vdots & \ddots \end{pmatrix} \begin{pmatrix} A^{(\text{ex},1)} \\ A^{(\text{in},1)} \\ A^{(\text{ex},2)} \\ A^{(\text{in},2)} \\ \vdots \end{pmatrix} = 0, \quad (28)$$

where all the definitions in Eq. (28) are as those of Paper I. Note that the dispersion relation is obtained by requiring that the system (28) has non-trivial solutions, i.e. its determinant is zero. In the next section, we solve the dispersion relation numerically to obtain the frequencies ω and damping rates γ of the resonantly damped MHD kink oscillations of longitudinally stratified elliptical emerging coronal loops.

4 Numerical Results

To solve the dispersion relation (28) numerically, we chose the physical parameters $L = 10^5$ km, $R/L = 0.01$, $l/R = 0.02$, $B = 100$ G, $\rho_{\text{in}} = 2 \times 10^{-14}$ g cm $^{-3}$ and $\rho_{\text{ex}}/\rho_{\text{in}} = 0.1$. For such a loop one finds $v_{A_{\text{in}}} = \frac{B}{\sqrt{4\pi\rho_{\text{in}}}} = 2 \times 10^3$ km s $^{-1}$ and $\omega_{A_{\text{in}}} := \frac{v_{A_{\text{in}}}}{L} = 0.02$ rad s $^{-1}$. In what follows, we illustrate our numerical studies in the three separate equilibrium cases containing (i) circle-arc emerged loop (ii) minor elliptical semi-emerged loop and (iii) minor and major elliptical loops.

4.1 Circle-arc emerged loop ($\epsilon = 0$, $\lambda \neq 0$)

The effect of stage of emergence of the tube on both the frequencies ω and damping rates γ are calculated by numerical solution of the dispersion relation, i.e. Eq. (28). In Figs. 1 and 2, the frequencies, damping rates and their ratio for the fundamental and first-overtone kink ($m = 1$) modes are plotted versus the stratification parameter μ for a circle-arc flux tube ($\epsilon = 0$) at various stages of emergence containing early stage emergence ($\lambda = 0.75$), semi-emerged ellipse ($\lambda = 0$) and late stage emergence ($\lambda = -0.75$). Figures 1 and 2 show that (i) for a given loop shape parameter λ , both frequencies ω_1 , ω_2 and their corresponding damping rates $|\gamma_1|$, $|\gamma_2|$ increase when the stratification parameter μ increases. (ii) For a given μ , both frequencies and damping rates increase when λ increases. For instance, for $\mu = 0.9$, the early stage emergence $\lambda = 0.75$ in comparison with late stage emergence $\lambda = -0.75$ would cause $\omega_1, \omega_2, |\gamma_1|$ and $|\gamma_2|$ to increase by about 10.2%, 11.7%, 10% and 14.5%, respectively. (iii) The ratio of the oscillation frequency to the damping rate, $\omega/|\gamma|$, is independent of stratification. Also the stage of emergence of the loop does not affect $\omega/|\gamma|$. This means that the ratio $\omega/|\gamma|$ is independent of how the loop center is situated with respect to the photosphere.

In Fig. 3, the ratio of the frequencies ω_2/ω_1 of the first overtone and its fundamental mode is plotted versus the stratification parameter. Figure 3 shows that (i) for a given λ , the frequency ratio decreases from 2 (for an unstratified loop) with increasing density stratification. (ii) For a given μ , the frequency ratio decreases when λ decreases. The results of ω_2/ω_1 are in agreement with those obtained by Morton & Erdélyi (2009).

4.2 Minor elliptical semi-emerged loop ($\epsilon \neq 0$, $\lambda = 0$)

Figures 4 and 5 as Figs. 1 and 2 display the result of frequency, damping rate and ratio $\omega/|\gamma|$ but for a minor semi-emerged loop ($\lambda = 0$) with different ellipticity parameters $\epsilon = 0.0, 0.4$ and 0.6 . Figures 4 and 5 show that (i) for a given ellipticity parameter ϵ , both frequencies ω_1 , ω_2 and their corresponding damping rates $|\gamma_1|$, $|\gamma_2|$ increase when the stratification parameter μ increases. (ii) For a given μ , both frequencies and damping rates increase with increasing ϵ . For instance, for $\mu = 0.9$ considering a loop with $\epsilon = 0.6$ would cause to increase $\omega_1, \omega_2, |\gamma_1|$ and $|\gamma_2|$ up to 3.5%, 4%, 3.5% and 5.3%, respectively, in comparison with a semi-circular loop ($\epsilon = 0$). (iii) The ratio $\omega/|\gamma|$ remains unchanged by increasing the stratification parameter. Also this ratio is independent of the elliptical shape of the loop.

Figure 6 illustrates the frequency ratio ω_2/ω_1 as a function of stratification parameter for a semi-emerged loop ($\lambda = 0$) with different ellipticity parameters. Figure 6 presents that (i) for a given ellipticity parameter, the ratio ω_2/ω_1 decreases from 2 by increasing the stratification parameter and approaches below 1.5. (ii) For a given μ , the frequency ratio ω_2/ω_1 decreases when ϵ decreases. This is in good concord with the result of Morton & Erdélyi (2009).

4.3 Minor and major elliptical emerged loops ($\epsilon \neq 0$, $\lambda \neq 0$)

Figures 7, 8 and 9 make it possible to do some comparisons between major and minor elliptical cases. Figures 7 and 8 show that: (i) the frequencies and damping rates of both fundamental and first-overtone kink ($m = 1$) modes of a minor elliptical case are greater than those of a major elliptical case and also of a circular-arc semi-emerged loop ($\epsilon = \lambda = 0$) studied in Paper I. For instance, for $\mu = 0.9$ for a minor elliptical loop with $\epsilon = 0.6$ and $\lambda = 0.75$, the values of ω_1 , ω_2 , $|\gamma_1|$ and $|\gamma_2|$ are 19.1%, 26.2%, 18.4% and 22.4% greater than those of a major elliptical case, respectively. (ii) The frequencies and damping rates of a major elliptical loop are slightly greater than the circular-arc semi-emerged loop. (iii) The ratio $\omega/|\gamma|$ of both fundamental and first-overtone modes do not affected by stratification for minor/major elliptical and circular-arc semi-emerged loops.

In Fig. 9, the frequency ratio ω_2/ω_1 versus the stratification parameter is plotted for major and minor cases as well as a circular-arc semi-emerged loop. Figure 9 shows that: (i) for a given μ , the frequency ratio ω_2/ω_1 of the minor elliptical loop is greater than the major one. For instance, for $\mu = 0.9$, the ratio ω_2/ω_1 of a minor elliptical case is 5.9% greater than that of a major elliptical one. (ii) The ratio ω_2/ω_1 in a major elliptical loop is slightly greater than the circular-arc semi-emerged loop. Therefore, the major ellipse has a lesser effect on the frequency ratio of standing kink oscillations. This is in good accordance with that obtained by Morton & Erdélyi (2009).

5 Conclusions

Here we investigated the effects of both ellipticity and stage of emergence on the resonant absorption of standing kink waves in longitudinally stratified coronal loops. We considered a coronal loop as a pressureless cylindrical flux tube embedded in a straight magnetic field that undergoes a longitudinal density stratification and radial density structuring. We extended the relevant connection formulae for the resonant absorption of transverse kink oscillations of a coronal loop with an elliptical shape, at various stages of its emergence from the sub-photosphere into the solar corona. We studied three stages of emergence of the loop at which the center of eclipse is sitting below ($\lambda > 0$), on ($\lambda = 0$), and above ($\lambda < 0$) the photosphere. We considered two types of elliptical loop that can occur, the minor ellipse and the major ellipse. Note that the minor ellipse is a situation that occurs most plausibly under coronal conditions. By numerically solving the dispersion relation, we obtained the frequencies and damping rates of the fundamental and first-overtone kink ($m = 1$) modes. Our numerical results show the following.

i) By increasing the density stratification parameter μ in the loop, both frequencies and damping rates increase while the frequency ratio ω_2/ω_1 decreases.

ii) In a circle-arc emerged loop ($\epsilon = 0$, $\lambda \neq 0$) for a given μ , the frequencies, damping rates and the frequency ratio increase when the stage of emergence parameter λ increases.

iii) In a minor elliptical semi-emerged loop ($\epsilon \neq 0$, $\lambda = 0$) for a given μ , the frequencies, damping rates and the frequency ratio increase when the ellipticity parameter ϵ increases.

iv) In a minor elliptical emerged loop ($\epsilon \neq 0$, $\lambda \neq 0$) for a given μ , the frequencies, damping rates and frequency ratio are greater than those of a major one. However, the results obtained for the aforementioned quantities in the major elliptical emerged loop are slightly greater than those of a circular-arc semi-emerged loop ($\epsilon = \lambda = 0$).

v) The ratio of the oscillation frequency to the damping rate, $\omega/|\gamma|$, in minor/major elliptical and circular-arc semi-emerged loops, is not affected by making changes in density stratification parameter, ellipticity and stage of emergence of the loop.

Acknowledgements

The work of K. Karami has been supported financially by Department of Physics, University of Kurdistan, Sanandaj, Iran under research project No. 1/1390.

References

- [1] Andries J., Arregui I., Goossens M., 2005a, ApJ, 624, L57
- [2] Andries J., Goossens M., Hollweg J.V., Arregui I., Van Doorselaere T., 2005b, A&A, 430, 1109
- [3] Aschwanden M.J., De Pontieu B., Schrijver C.J., Title A.M., 2002, Sol. Phys., 206, 99
- [4] Aschwanden M.J., Fletcher L., Schrijver C.J., Alexander D., 1999, ApJ, 520, 880
- [5] Davila J.M., 1987, ApJ, 317, 514
- [6] Dymova M.V., Ruderman M.S., 2006, A&A, 457, 1059
- [7] Erdélyi R., Goossens M., 1994, Ap&SS, 213, 273
- [8] Erdélyi R., Goossens M., 1995, A&A, 294, 575
- [9] Erdélyi R., Verth G., 2007, A&A, 462, 743
- [10] Goossens M., Terradas J., Andries J., Arregui I., Ballester J.L., 2009, A&A, 503, 213
- [11] Ionson J.A., 1978, ApJ, 226, 650
- [12] Karami K., Asvar A., 2007, MNRAS, 381, 97
- [13] Karami K., Barin M., 2009, MNRAS, 394, 521
- [14] Karami K., Nasiri S., Amiri S., 2009, MNRAS, 394, 1973 (Paper I)
- [15] Karami K., Bahari K., 2010, Sol. Phys., 263, 87
- [16] Karami K., Bahari K., 2012, ApJ, 757, 186
- [17] Morton R.J., Erdélyi R., 2009, A&A, 502, 315
- [18] Nakariakov V.M., Ofman L., DeLuca E.E., Roberts B., Davila J.M., 1999, Science, 285, 862
- [19] Ofman L., Aschwanden M.J., 2002, ApJ, 576, L153

- [20] Ofman L., Davila J.M., Steinolfson R.S., 1994, *ApJ*, 421, 360
- [21] Poedts S., Goossens M., Kerner W., 1989, *Sol. Phys.*, 123, 83
- [22] Safari H., Nasiri S., Karami K., Sobouti Y., 2006, *A&A*, 448, 375
- [23] Safari H., Nasiri S., Sobouti Y., 2007, *A&A*, 470, 1111
- [24] Schrijver C.J., Brown D.S., 2000, *ApJ*, 537, L69
- [25] Tirry W.J., Goossens M., 1996, *ApJ*, 471, 501
- [26] Van Doorselaere T., Nakariakov V.M., Verwichte E., 2007, *A&A*, 473, 959
- [27] Verth G., Erdélyi R., Jess D.B., 2008, *ApJ*, 687, L45
- [28] Verwichte E., Nakariakov V.M., Ofman L., Deluca E.E., 2004, *Sol. Phys.*, 223, 77

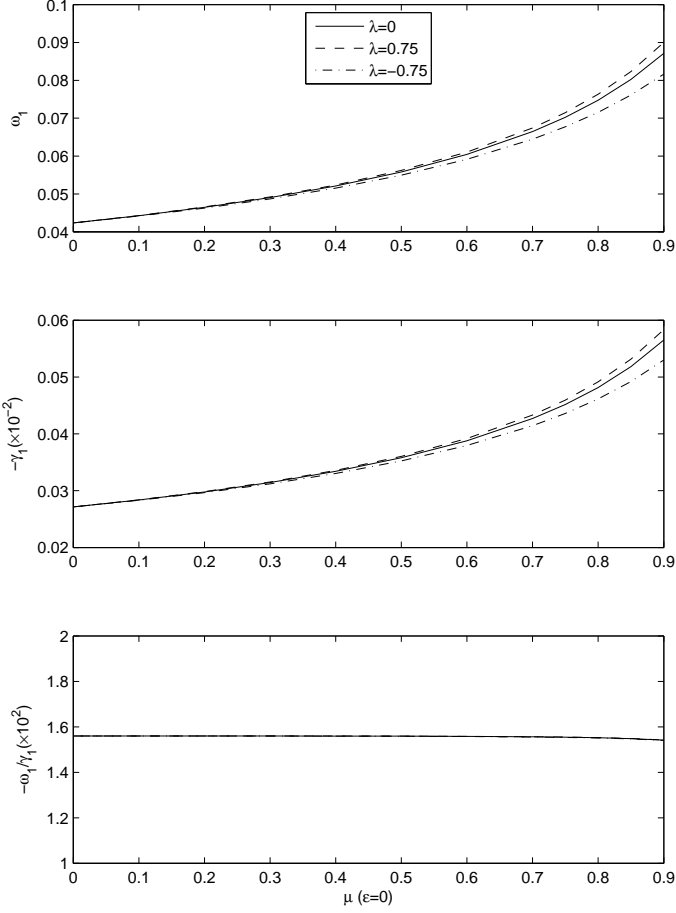


Figure 1: Frequency of the fundamental kink ($m = 1$) mode and its damping rate as well as the ratio of the oscillation frequency to the damping rate as a function of the stratification parameter μ for a circle-arc flux tube ($\epsilon = 0$) at various stages of emergence $\lambda = 0$ (solid), 0.75 (dashed) and -0.75 (dash-dotted). The loop parameters are $L = 10^5$ km, $R/L = 0.01$, $l/R = 0.02$, $\rho_{\text{ex}}/\rho_{\text{in}} = 0.1$, $\rho_{\text{in}} = 2 \times 10^{-14}$ gr cm^{-3} and $B = 100$ G. Both frequencies and damping rates are in units of the interior Alfvén frequency, $\omega_{\text{Ain}} = 0.02$ rad s^{-1} .

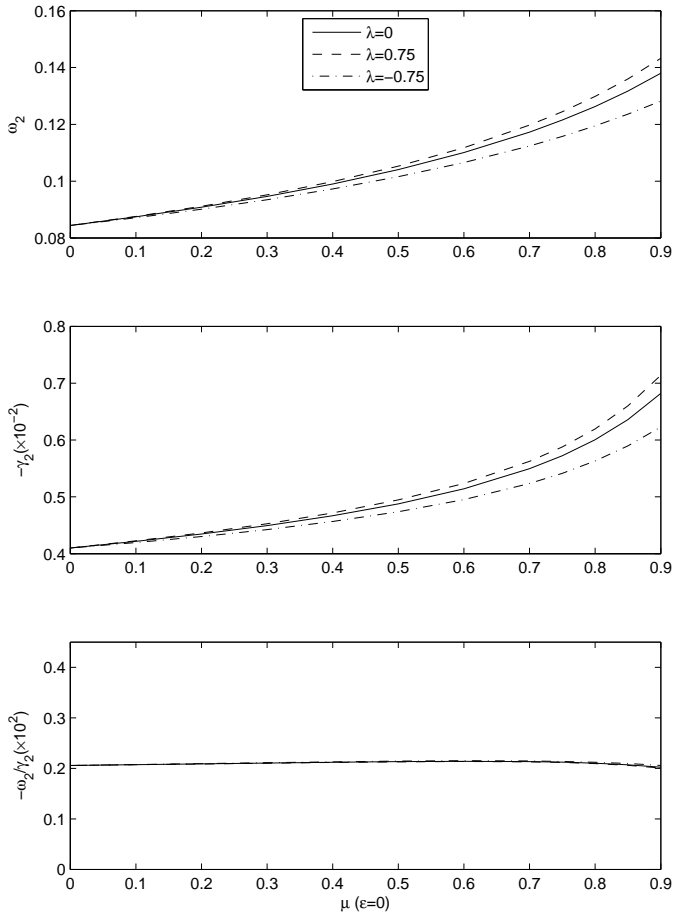


Figure 2: Same as Fig. 1, for the first-overtone kink modes.

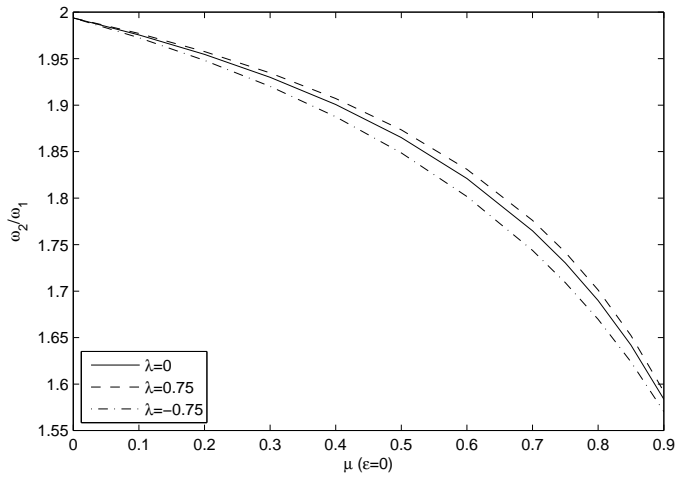


Figure 3: Ratio of the frequencies ω_2/ω_1 of the first-overtone and its fundamental kink ($m = 1$) mode versus μ for a circle-arc flux tube ($\epsilon = 0$) at various stages of emergence $\lambda = 0$ (solid), 0.75 (dashed) and -0.75 (dash-dotted). Auxiliary parameters as in Fig. 1.

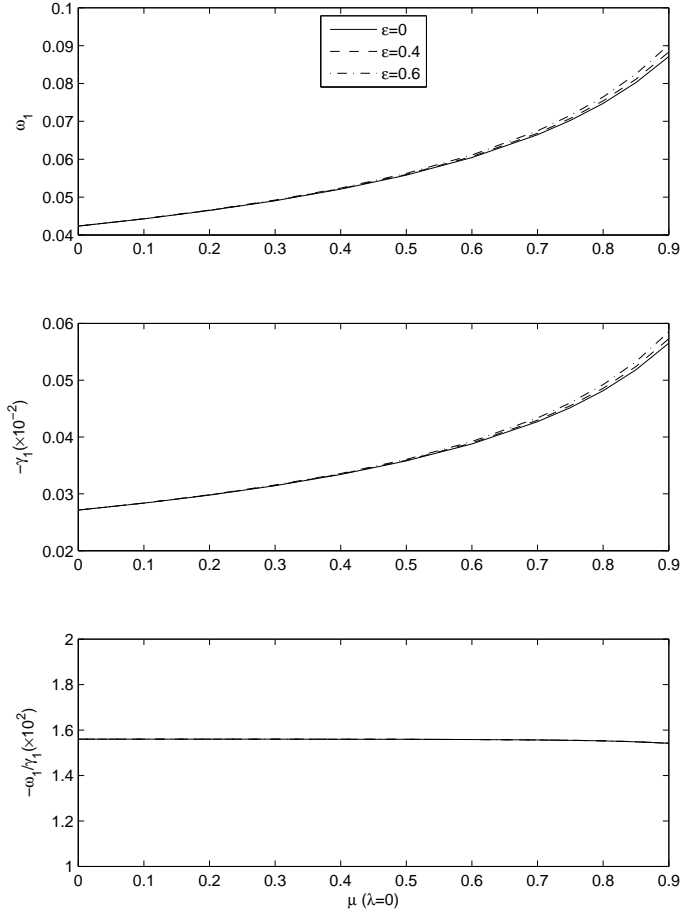


Figure 4: Frequency of the fundamental kink ($m = 1$) mode and its damping rate as well as the ratio of the oscillation frequency to the damping rate as a function of the stratification parameter μ for a minor semi-emerged loop ($\lambda = 0$) with different ellipticity parameters $\epsilon = 0.0$ (solid), 0.4 (dashed) and 0.6 (dash-dotted). Auxiliary parameters as in Fig. 1.

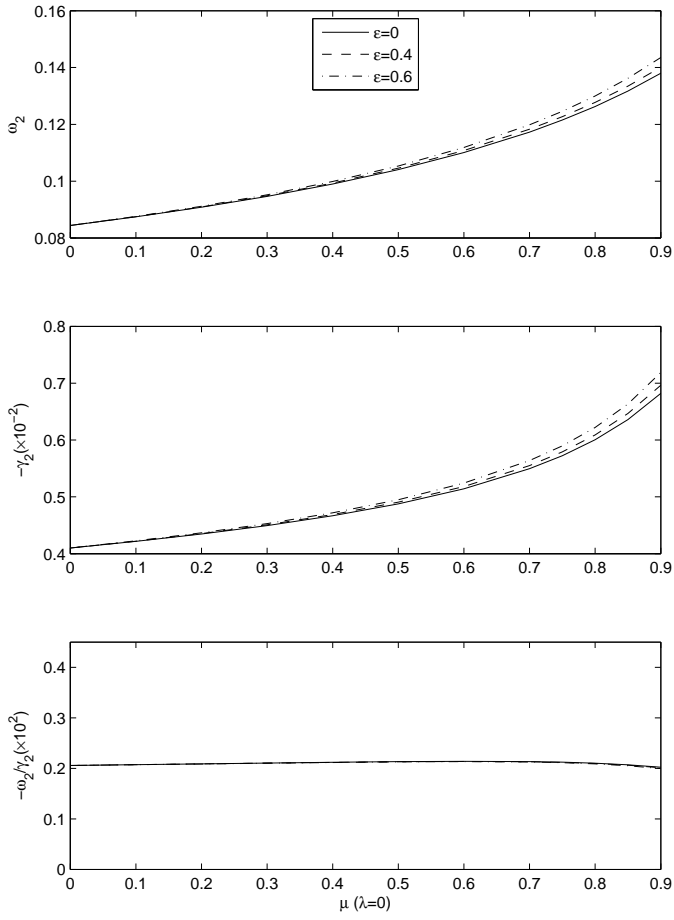


Figure 5: Same as Fig. 4, for the first-overtone kink modes.

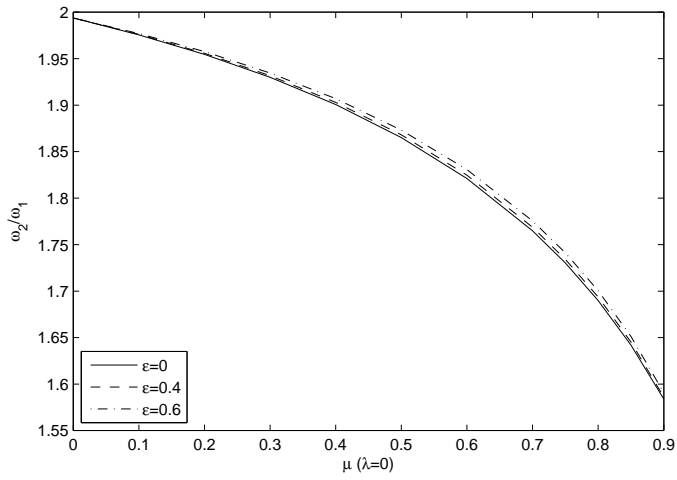


Figure 6: Ratio of the frequencies ω_2/ω_1 of the first-overtone and its fundamental kink ($m = 1$) mode versus μ for a minor semi-emerged loop ($\lambda = 0$) with different ellipticity parameters $\epsilon = 0.0$ (solid), 0.4 (dashed) and 0.6 (dash-dotted). Auxiliary parameters as in Fig. 1.

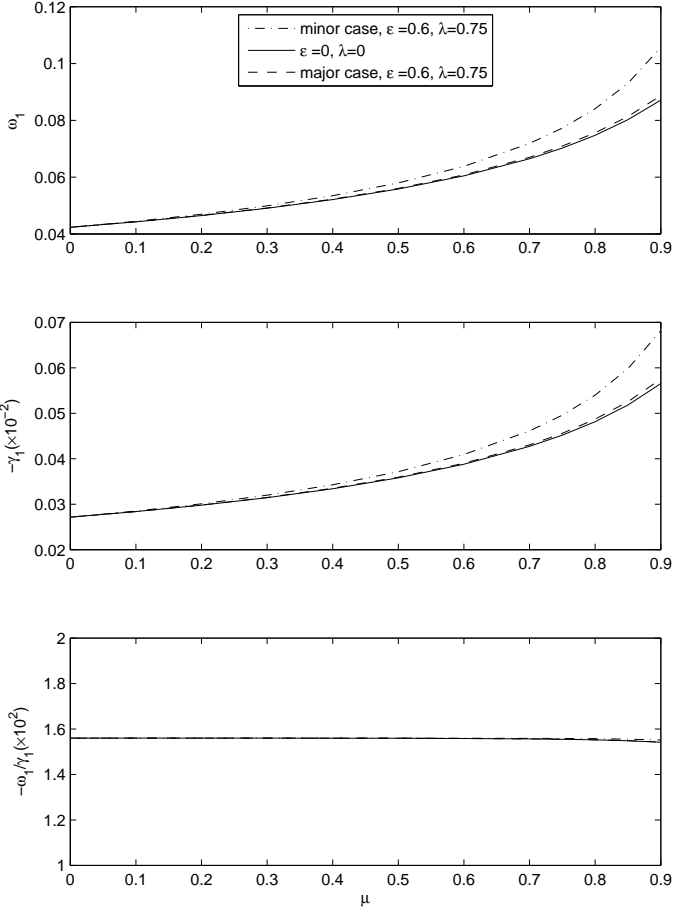


Figure 7: Frequency of the fundamental kink ($m = 1$) mode and its damping rate as well as the ratio of the oscillation frequency to the damping rate as a function of the stratification parameter μ for circular-arc semi-emerged (solid), minor (dash-dotted) and major (dashed) elliptical loops. Auxiliary parameters as in Fig. 1.

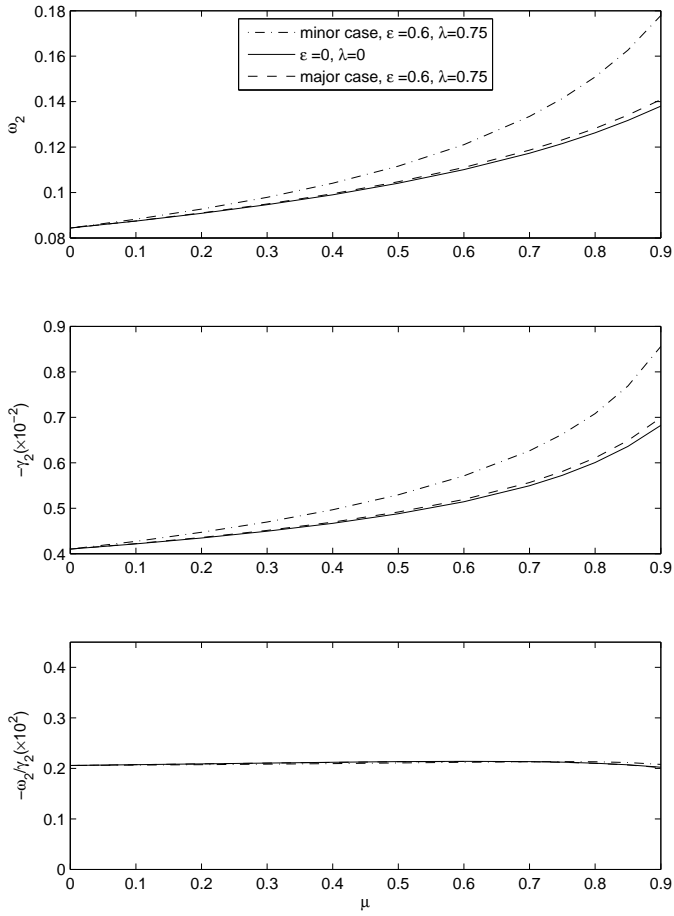


Figure 8: Same as Fig. 7, for the first-overtone kink modes.

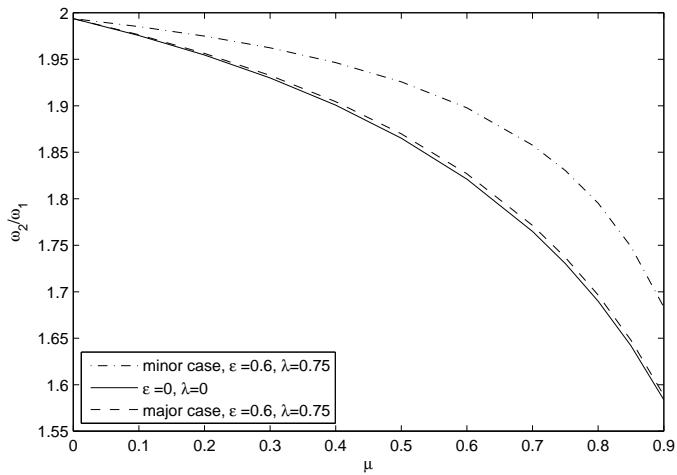


Figure 9: Ratio of the frequencies ω_2/ω_1 of the first-overtone and its fundamental kink ($m = 1$) mode versus μ for circular-arc semi-emerged (solid), minor (dash-dotted) and major (dashed) elliptical loops. Auxiliary parameters as in Fig. 1.